Received: 5 March 2021 | Revised: 5 August 2021 | Accepted: 30 August 2021

DOI: 10.1002/cpe.6631

RESEARCH ARTICLE

WILEY

Artificial intelligent based smart system for safe mining during foggy weather

Sushma Kumari | **Monika Choudhary** | **Richa Mishra** | **Swades Kumar Chaulya** | **Girendra Mohan Prasad** | **Sujit Kumar Mandal** | **Gautam Banerjee**

Mine Mechanization, Automation, and Technology Development Group, CSIR-Central Institute of Mining and Fuel Research, Dhanbad, Jharkhand, India

Correspondence
Sushma Kumari, Mine Mechanization, Automation, and Technology Development Group, CSIR-Central Institute of Mining and Fuel Research, Dhanbad 826001, Jharkhand, India.
Email: kumarisushma7870@gmail.com

Funding information
Ministry of Electronics and Information Technology; CSIR-Central Institute of Mining and Fuel Research; National Mineral Development Corporation Limited, Hyderabad, India

Abstract

Opencast mining operations at hilly areas are usually affected during foggy weather due to the inability of drivers to operate heavy earth-moving machinery in low visibility conditions. This article deals with an intelligent vision enhancement system for continuing opencast mining operations during foggy weather. The system integrates hardware and software to provide multistage safety features that make it unique from existing systems. The system includes hardware like thermal cameras, high definition cameras, proximity radar, wireless devices, GNSS module, graphical processing unit, display unit, and so forth, and image processing software, namely real-time image stitching, image enhancement, and object detection using convolutional neural networks. The integrated system and algorithms display a 180° panorama field view of the vehicle's front using real-time video stitching. The front view after image processing, rear camera view, object detection through proximity radar, and real-time location of the vehicles on a 3D geo-tagged mine map by GNSS modules are displayed in four splitter windows on a touch screen fitted on the dashboard in front of the driver's seat. The driver can drive the vehicle by seeing the display screen during foggy weather. The output image of the developed image-processing algorithm has less distortion, better quality, and better depth perception than existing methods. Overall, there are significant improvements in the persistence of the color elements by 39.65%, contrast by 4.62%, and the corresponding entropy by 7.11% concerning the similar existing methods. The final system has been successfully tested in an opencast mine.

KEYWORDS

convolutional neural network, defogging, foggy image, object detection, real-time video processing

1 | INTRODUCTION

Driving heavy earth-moving machinery (HEMM) in opencast mines during unfavorable weather conditions poses difficulty to operators as the visibility is significantly reduced by fog, feeble light surroundings, smoke, dust particles, and rain.[1,2] A system has been developed by installing high-definition/thermal cameras in the front and rear of HEMM and displaying the real-time panorama view of the road in front and back of HEMM on the screen fitted on a dashboard in front of the driver to continuing mining operations during foggy weather. The driver can drive HEMM by watching the front and rear view of the road on the screen. However, the displayed real-time image on the screen without image processing is unclear due

to foggy weather. Predominantly, contrast, color, and visibility features of real scenes are affected by foggy weather. Real-time image processing is the best tool to solve such problems to remove fog from the image and better visibility of vehicle drivers during foggy weather. Hence, some of the existing image processing techniques have been studied to suit real-time image processing.

For image enhancement, the contrast of the foggy image can be restored using the dark channel prior (DCP) method and Gamma adjustment in the histogram of the affected images.[3–6] This method estimates the transmission ratio of atmospheric light and then adjusts the histogram of images accordingly using the Gamma transform. It captures the same scene under different weather conditions to generate a transmission ratio map, which is not feasible for real-time image processing. The calculation is complex and time taking for the instant situation. Many researchers have studied different image defogging techniques using various filters have been reviewed by many researchers[7,8] using a high-booster, homomorphic filter, Weiner filter, and discrete wavelet transformations (DWT) to enhance foggy images. Based on statistical analysis, it has been reported that DWT outperformed other filters.[7] According to Qiu et al.,[9] contrast limited adaptive histogram equalization (CLAHE) is one of the most appropriate and efficient image processing parameters to automatically determine the required contrast of the image. They have used the CLAHE method to enhance the contrast of a 2D X-ray image for medical purposes. For the enhancement of medical images, many other researchers have also used CLAHE for contrast enhancement. Koonsanit et al.[10] have applied CLAHE for digital X-ray image enhancement. Maxwell et al.[11] recommended that CLAHE is an ideal image enhancement technique for a sclera blood vessel. Bandara et al.[12] explained the image enhancement technique for superficial vein imagery using CLAHE. For medical image enhancement, CLAHE is the most used technique for contrast restoration, but it adversely affects an image's color elements.[13]

Ma et al.[14] and Ramya et al.[15] have used CLAHE for foggy as well as underwater image and video enhancement. The mixed image enhancement technique using both CLAHE and DWT has been used for foggy image enhancement.[3,16] Kim et al.[17] have explained a hybrid technique for foggy image enhancement of indoor and outdoor environments. This method includes DCP followed by CLAHE and DWT for overall contrast enhancement and virtual histogram stretching of an image. The DCP method estimates atmospheric light's thickness and extracts it for a haze-free image.[5,18,19] The DCP method gives excellent results regarding the image's contrast, but it destroys its actual color. Above-mentioned approaches only enhance features of the specified portion and some aspects of the image, but it also creates noise and color distortion. Thus, there is a requirement for an effective system and real-time image processing technique that can provide the road's indistinct view to the driver and operator of HEMM to continue opencast mining operations during foggy weather to reduce the threat of transportation accidents.

This article proposes a multistage safety system to assist HEMM operators in driving efficiently without any hindrance caused by fog and continue opencast mining operations during foggy weather. Compare to other existing systems, the proposed system has been designed by integrating long-range proximity radar, GNSS devices, thermal and HD cameras, wireless devices, graphical processing unit (GPU), and image processing technology.

Combining image processing and other devices will help the operators drive during those unfavorable weather conditions by removing the fog from an image and displaying the real-time images on a dashboard screen in front of the driver's seat. When any other vehicles come nearby, the system generates an alarm to mitigate the possible threat of vehicle collision and make the system more reliable during adverse weather conditions.

Apart from mentioned devices, the system incorporates effective image processing techniques (real-time image stitching, image enhancement, and object detection through a convolutional neural network). All algorithms are merged to form a final output image presented in front of the driver's seat. The final image uses three cameras to provide a dehaze 180° panorama view; the drivers can see through the fog and detect the object with a clear path view. Artificial intelligence technology has been used for object detection and warning drivers. The merged algorithm has been finally deployed in the system through a high-speed GPU for real-time application. The final output of all the devices and processing software are displayed in four splitter windows on a screen fitted in front of the driver seat of a dumper covering the front and rear views of the road, GNSS-based navigation on a 3D geo-tagged mine map, and radar-based proximity view with a warning. The developed system has also been deployed in different HEMM of an opencast mine to form a whole system capable of providing a clear view of the road to drive during foggy weather with improved visibility.

This article proposes a real-time image enhancement technique called CLAHE with the image sharpening and color correction (CISACC) method to enhance visibility. In the CISACC method, the conventional CLAHE method has been used to enhance contrast, followed by image sharpening and color correction to emphasize the features and veracious color of the image. The proposed algorithm firstly works for fog removal by applying CLAHE on the value channel among the image's hue, saturation, and value (HSV) color space. Then, it works for accentuating the features using a high pass spatial filter of 3×3 kernel size. The image's due to much virtual histogram stretching and filtering through CLAHE and sharpening. The distortion of the processed image has been corrected using the color correction algorithm. The article describes the developed vision enhancement system as well as image stitching, CISACC, and object detection methods. The technology was tested in an opencast mine and yielded a better result than existing normal CLAHE and DCP, AOD-Net,[20] and FFA-Net[21] methods.

The article incorporates the architecture of the vision enhancement system for deployment in HEMM of opencast mines, description of the proposed CISACC image enhancement algorithm, performance analysis of the proposed algorithms by conducting field trials in an opencast mine during foggy weather, and comparison of the test results with other existing algorithms.

2 | SYSTEM ARCHITECTURE

Figure 1 shows the developed vision enhancement system's architecture installed on a HEMM of an opencast mine. The whole system consists of a framework of hardware and software. The hardware includes internet protocol (IP) thermal and high definition (HD) cameras, proximity radar, global navigation satellite system (GNSS), anticollision laser light, retro-reflective materials, graphical processing unit (GPU), display unit, wireless devices, and other roadside edge detection apparatus like a flashlight, self-regulating heating cable, retro-reflecting material, and so forth. The software module includes the integrated image processing algorithms (image stitching, image enhancement, and object detection using convolutional neural network) deployed in a GPU, radar-based proximity warning software, GNSS-based navigation software, fleet management software, and so forth. The thermal imagining camera assists the drivers in seeing through dust, even in dense fog, haze, and low light conditions like night-time. As the field of view of one camera is not sufficient to cover the wanted area, three IP cameras are installed on the front of the vehicle to provide a 180° field of view using an image stitching algorithm. A camera is mounted on the vehicle's rear end to give the operators a rear view of the road when operating a HEMM in the opencast mine (Figure 2). The camera's input image first goes through the set of integrated algorithms, and the final output is displayed on the display board fitted on the front of the driver seat. The final processed image can provide a dehazed image and detect any obstructions on the operator's path. The proximity radar is also installed on the front side of the vehicle having a detection range of 50 m; when any obstacles are present within the radar range, the system can detect the obstacle. It warns the driver regarding the potential threat of vehicle collision by providing an audio-visual alarm displayed through the dashboard screen fitted on the vehicle. The system also includes a GNSS module installed on the vehicle's front to locate its accurate position and proximity awareness of other near vehicles on the 3D geo-tagged mine map. The system also provides fleet management software for optimum utilization of shovel-dumper combination in an opencast mine.

This system helps the operators find their exact location and warn when a surrounding vehicle is detected lesser than the safe distance. The GNSS data transceiver transmits vehicle position to the nearest base station and simultaneously receives other vehicles' positions inside mine premises onto its dashboard. All the processed output of the IP camera, proximity radar, and GNSS module have been integrated on a 16-inch touchscreen display board mounted on the driver seat's front. The display board was further split into four sections to represent each independent function, as shown in Figure 2. The top half displays the output of integrated algorithms applied to three IP cameras. The lower section is divided into proximity radar view, GNSS-based navigation on a 3D geo-tagged mine map, and the road's rear side. The drivers can select any particular section using a touch panel to display on full screen, while the other sections continue to run in the background and pop up an alert when necessary. A network switch is used for the terminal connection of all Ethernet-based modules such as cameras, proximity radar, and GNSS. Finally, a rugged PC or GPU is used to process all the cameras, proximity radar, GNSS information, and other mentioned software. The power required to run the whole system is derived from the vehicle only.

In addition to the above equipment, some other devices are also incorporated with the system, like self-regulating heating cables, retro-reflective material, anticollision laser light, and flasher light. Retro-reflective material is primarily used to increase night-time views of traffic signs, road surfaces, vehicles, etc. Anti-collision laser light is installed on the vehicle's rear end to warn the other operator behind it and avoid traffic accidents while driving in the rain, fog, and low light conditions. Further, the self-regulating heating cables are laid on some parts of road edges to properly detect the sharp turns for the operators through thermal cameras while driving HEMM during foggy weather conditions. Hence, the developed system provides multilayered protection and visualization of mining operations using different techniques to enhance the operators' visibility. For further analysis, a comparative study of the proposed system with other existing driving assistance systems,[22–27] is given in Table 1.

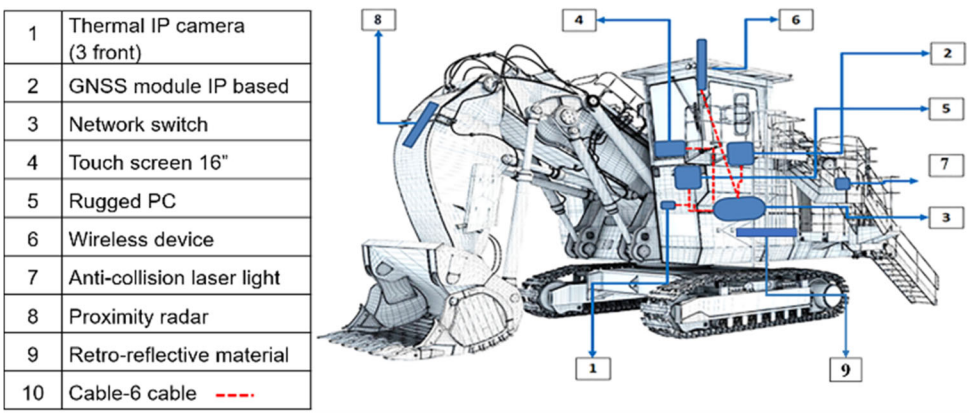

FIGURE 1 System architecture

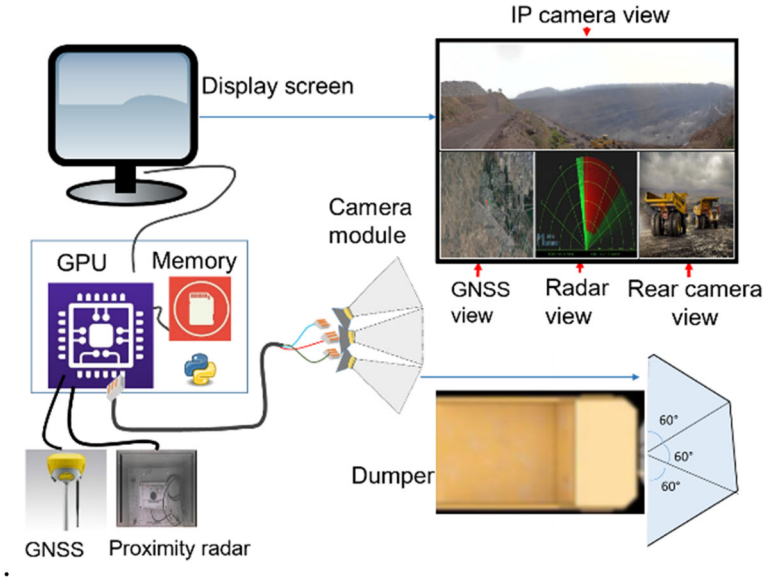

FIGURE 2 Installed three cameras on the dumper's front and image stitching, processing, and displaying on a screen

TABLE 1 Comparative analysis of the proposed system with the existing driving assistance system

Technology used		Nieto et al.[22]	Sun and Zhang[23]	Spinneker et al.[24]	Nieto et al.[25]	Ruff[26]	Xiao et al.[27]	Proposed system
Hardware	Thermal camera	×	✓	×	×	×	×	✓
	HD camera	×	×	✓	×	✓	×	✓
	Proximity radar	×	×	×	×	✓	×	✓
	GNSS/GPS	✓	✓	×	✓	×	×	✓
	Anti-collision laser light	×	×	×	×	×	×	✓
	Self-regulating heating cable	×	×	×	×	×	×	✓
	Wireless networking	✓	×	×	✓	×	✓	✓
Software	Image stitching	×	×	×	×	×	×	✓
	Image enhancement	×	✓	✓	×	×	×	✓
	Object detection	×	✓	×	×	×	×	✓
	GNSS based proximity awareness	✓	✓	×	✓	×	×	✓
	Radar-based proximity warning	×	×	×	×	✓	×	✓
	Vehicle tracking software	×	✓	×	✓	×	×	✓
	Navigation using 3D geo-tagged mine map	✓	✓	×	✓	×	×	✓
	Fleet management software							
	• Production monitoring	×	×	×	×	×	×	✓
	• Geofencing	×	×	×	×	×	×	✓
	• Optimization of shovel and dumper performance	×	×	×	×	×	×	✓
	• Trip count	×	×	×	×	×	×	✓

The proposed system has backup security measures like proximity radar, GNSS-based navigation, anticollision laser light, and so forth, apart from visibility enhancement algorithms. It minimizes road accidents by reducing human error and improves productivity using fleet management software. The designed system enhances the visibility of the driver. It avoids accidents and collisions by offering technologies that warn the driver of incoming obstacles.

The entire system has been tested and deployed in an opencast mine (Bacheli Complex, Bailadila Iron Ore Mine, India) for safe driving during harsh weather conditions. Earlier, mining operations could not be carried out during the rainy season due to very dense fog for around 50–60 days in a year and the possibility of accidents and vehicles collisions.

3 | PROPOSED IMAGE PROCESSING ALGORITHM

Figure 3 shows the framework of the proposed image processing algorithm. The algorithm contains three real-time image processing techniques, that is, real-time video stitching of three cameras, image enhancement, and object detection. An image stitching algorithm has been applied to provide a 180° field of view to HEMM. The continuous frames captured by the three identical cameras act as an input frame for the algorithm, then after keypoints detection, all the frames have been marked for further matching the same key points. After sorting the well-matched key points, homography matrices are generated for mosaicking the frames and then wrapped into a perspective projection for similar alignment.

The object detection algorithm consists of a neural network model trained on a custom dataset. A pretrained model, that is, SSD_MobileNet, has been selected for its accuracy and the dataset consists of 11 classes, mainly heavy vehicles available in mine sites. The model includes different neural network layers, and each layer has its function. The layer consists of feature extraction, localization, and detection layer to detect the objects' classes. An image enhancement method has been used to reduce the fog named CLAHE with the image sharpening and color correction (CISACC) algorithm.

The CISACC algorithm consists of four steps: color space conversion, CLAHE filtering, image sharpening, and color correction. The color space of the target image has been tested using the CLAHE filter. It has been observed that HSV is the best-fitted color space for CLAHE as it increases visibility to a reasonable extent after filtering. The HSV color space separates the image's hue channel, saturation channel, and intensity value channel. The CLAHE is applied only to the image's value channel so that the color elements of the image do not get altered.[14]

3.1 | CLAHE filtering

It is the method of adaptive histogram equalization, where the image is divided into different tiles, and the histogram is equalized for each tile locally. However, still, the contrast is uneven as the occurrence of gray intensity pixels is uneven. In CLAHE, pixel frequencies are clipped with a fixed predefined limit. The clip limit is decided according to the visibility of the image (Figure 4). Figure 4A shows the histogram with a higher variable frequency, and Figure 4B illustrates the histogram after clipping the frequency within a limit.

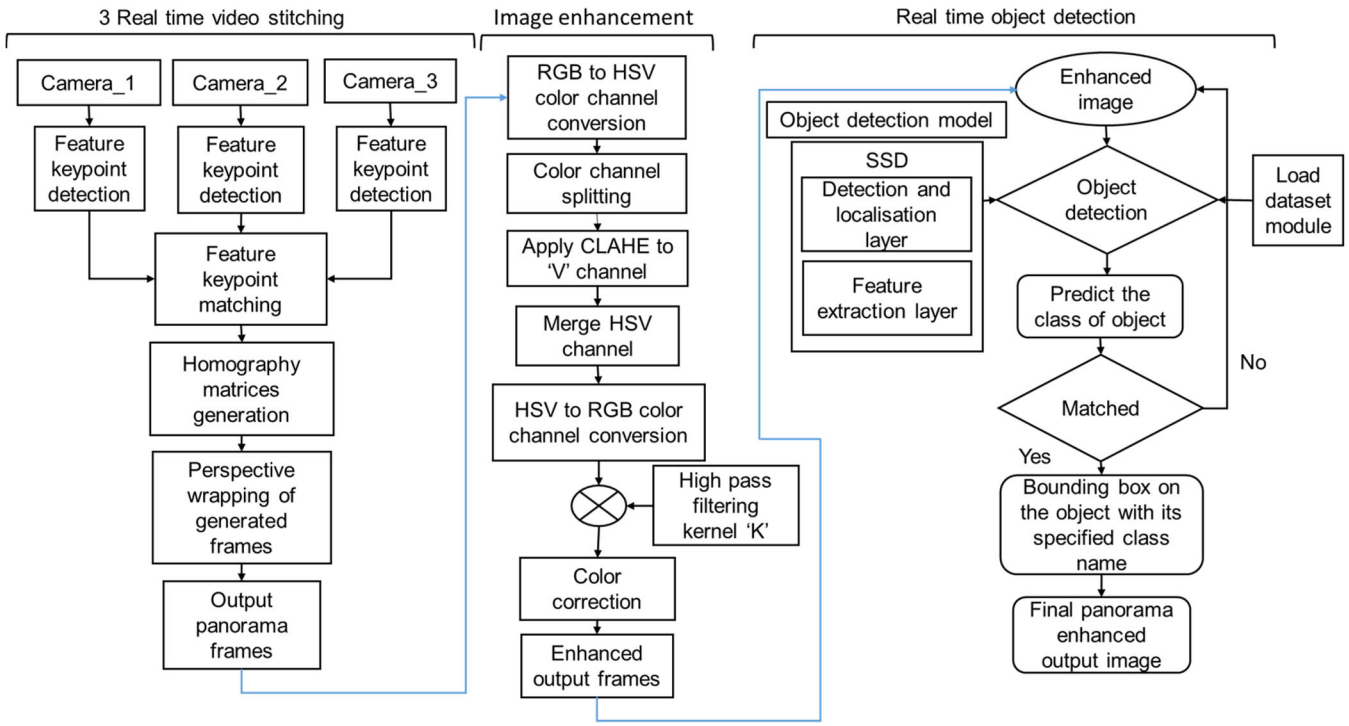

FIGURE 3 Intelligent vision enhancement method for real-time image stitching, image enhancement, and object detection

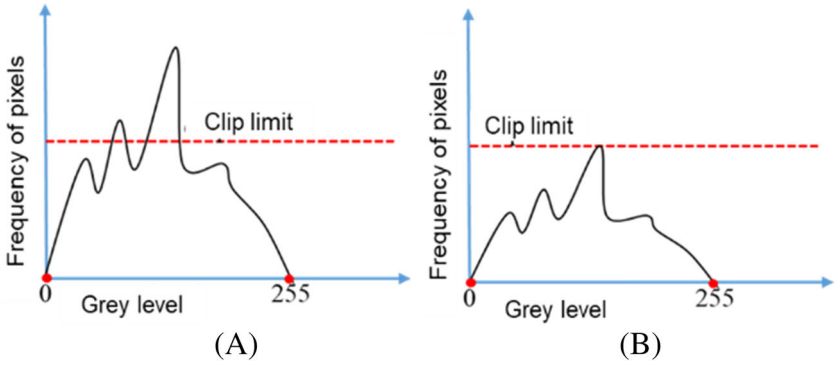

FIGURE 4 CLAHE clipping limit, (A) before clipping, and (B) after clipping

3.2 | Image sharpening

The perception of the human eye is susceptible to fine lines and feature points. A high pass filtering of 3×3 kernel size has been used to emphasize the image features. The kernel is represented by "k," where, $k = \begin{bmatrix} 0 & -0.5 & 0 \\ -0.5 & 3 & -0.5 \\ 0 & -0.5 & 0 \end{bmatrix}$.

Further, sharpening operation is represented as:

$$f(x) = [x]_{mxn} \otimes k, \tag{1}$$

where $[x]_{m \times n}$ are original pixels of $m \times n$ the matrix. The original image convolves with "k" to get a sharp image.

3.3 | Color correction

After defogging and sharpening, the image may have different local color tones and may suffer from lousy color contrast that must be corrected as they cause color distortion. The color correction algorithm mainly includes three steps:

1. Determining each channel histogram (i.e., red, green, and blue) and obtaining the minimum and maximum values of the histogram.
2. Removing the outlying values by saturating the specified percentage of pixels to black and white.
3. Saturating the histogram to span the ample range (i.e., 0–255).

Figure 5A,B have histograms of both the original and corrected images.

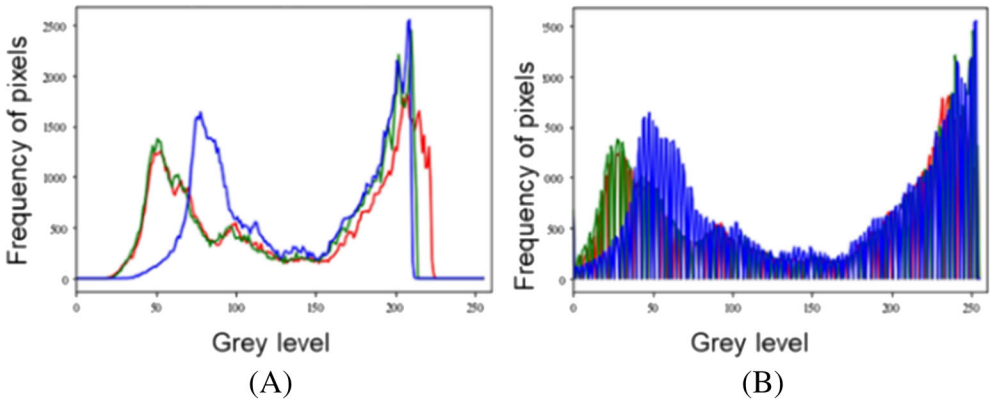

FIGURE 5 Transformation histogram, (A) before color correction, and (B) after color correction

(A)

(B)

FIGURE 6 Image stitching, (A) three camera views, and (B) final panoramic stitched image

It has been observed that the original histogram has a limited span of 37–230, and the corrected image has an entire span from 0 to 255 of the gray level. According to Limare et al.,[28] for saturating the histogram, affine transform has been used in each channel of the image, and the corrected image is represented by "*x*":

$$f(x) = ax + b, \tag{2}$$

where "*x*" is the image channel that must be saturated, "*a*" is the minimum saturation value (i.e., 0), and '*b*' is the maximum value (i.e., 255).

4 | EXPERIMENTAL RESULTS

4.1 | Real-time image stitching

The performance of the image stitching algorithm has been tested at an opencast mine for actual implementation. Three cameras and a GPU processor inbuilt with an image stitching algorithm have been installed in the vehicle to perform the real-time stitching and provide a 180° field of view to the driver.

Figure 6 shows the resultant final output of the stitched image, which indicated the algorithm's successful execution. The image stitching algorithm has been implemented on Python programming language and conducted on a GPU for its high-speed computation.

4.2 | Image enhancement

The output images of the system have been demonstrated using different test images. All the test images have been acquired from an opencast mine during foggy weather. Some of the processed images have been illustrated in Figure 7. Figure 7A represents the original image, which has been

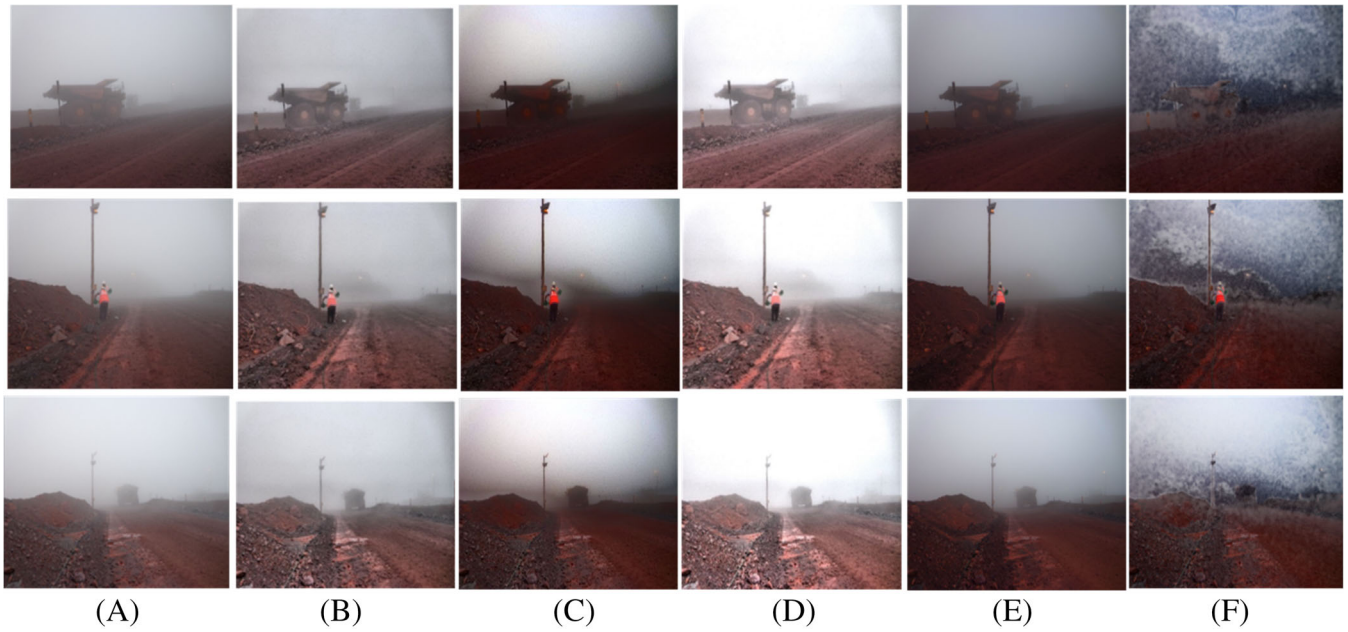

FIGURE 7 Test results of three images, (A) original image, (B) normal CLAHE filtered image, (C) DCP Images, (D) CISACC images, (E) AOD-Net images, and (F) FFA-Net images

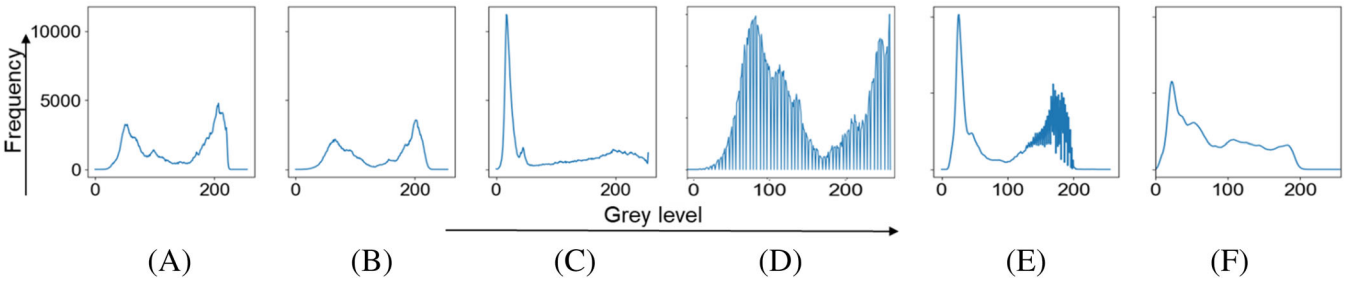

FIGURE 8 Test results histograms, (A) original image histogram, (B) normal CLAHE filtered image histogram, (C) DCP processed image histogram, (D) CISACC method image histogram, (E) AOD-Net image histogram, and (F) FFA-Net image histogram

further processed using the Python programming language. The output images of normal CLAHE, DCP, the proposed CISACC methods, AOD-Net, and FFA-Net have been depicted in Figure 7B–F. It has been observed that the CISACC method performed better than the other methods to preserve the actual color and visibility.

The histogram of a digital image is the spatial distribution of pixels according to their intensity. The histogram of a good contrast image has a gray level span of 0–255. Zero represents black, usually shown on the left side, and 255 denotes white, displayed on the right side of the histogram in the x-axis.[29]

Figure 8A indicates the histogram of the original input image. Histogram of the original image has been clipped by some amount, representing the usual CLAHE method as shown in Figure 8B. Whereas, Figure 8C depicts the histogram of the DCP processed image. Figure 8D implies the histogram of the proposed CISACC method, which clearly shows that it covers the whole span from 0 to 255 gray levels with clipping of excess intensity level locally. Figure 8E,F shows the histogram of the AOD-Net and FFA-Net algorithms.

4.3 | Object detection using CNN

Several test images of opencast mines were collected to evaluate the effectiveness of the developed algorithm. The k-fold cross-validation has been used to calculate the accuracy of model.[30] Figure 9 depicts the performance of the detector window of object detection using convolutional neural networks (CNN) for the opencast mine vehicles and miners working close to each other to be robustly detected. Object detection accuracy is 97%, which is displayed on the top of the bounding box and the object name (Figure 9).

FIGURE 9 Test results of object detection using CNN

5 | PERFORMANCE ANALYSIS AND DISCUSSION

Several parameters have been tested on the six original foggy images to evaluate the CISACC method's performance. The different performance criteria include natural image quality evaluation (NIQE), transmission and depth map estimation, cumulative distribution function, processing time taken by the algorithm, contrast, color average, entropy, and the number of feature key points. These performance parameters were evaluated for the CISACC, CLAHE, DCP, AOD-Net, and FFA-Net methods. The output values of the respective parameters were compared to assess the effectiveness of the CISACC with respect to other methods.

5.1 | Natural image quality evaluation

According to Mittal et al.,[31] NIQE is a type of no-reference image quality assessment (IQA) that automatically predicts the image's quality based on simple, special domain natural scene statistical (NSS) analysis. The quality of the image is expressed as the distance between the quality-aware NSS feature model and the multivariate Gaussian (MVG) suitable to the features extracted from the distorted image, which is represented as:

$$D\left(v_1, v_2, \sum_1, \sum_2\right) = \sqrt{\left((v_1 - v_2)^T \left(\frac{\sum_1 + \sum_2}{2}\right)^{-1} (v_1 - v_2)\right)}, \tag{3}$$

where D is the distance between the MVG of the test images and that of natural images, v_1, v_2 are mean vectors, and $\sum_1$, $\sum_2$ are covariance matrices of the natural and distorted images of the MVG model.

It is a process of constructing a quality-aware collection of statistical features based on a simple and successful space domain NSS model. These features are derived from a corpus of natural and undistorted images. The distorted image quality is expressed as a simple distance metric between the model statistics and those of the distorted image, so the lower the value of NIQE better the image quality.[32] NIQE value has been calculated for the different methods compared with the proposed CISACC method (Table 2).

It has been observed that the CISACC method has the lowest NIQE value among all compared methods (Figure 10). The NIQE value of CISACC is 13.51, and the DCP has the highest value of 32.30 (Table 2). This indicates that the output image by the CISACC method has lesser distortion and better quality than the existing CLAHE, DCP, AOD-Net, and FFA-Net methods.

5.2 | Transmission and depth map estimation

To extract the haze-free image, He et al.[33] introduced a method that includes extracting the haze-free image through a dark channel prior.

TABLE 2 Natural image quality evaluator value for different methods

Image type	NIQE value					
	Original	CLAHE	DCP	CISACC	AOD-Net	FFA-Net
Truck	13.916	14.84	25.779	14.345	14.557	18.286
Road	12.096	16.186	35.389	12.983	13.549	17.382
Man	12.654	13.908	37.633	13.398	13.939	15.987
Electric pole	13.754	15.432	28.693	13.843	14.673	16.209
Miner	13.432	14.645	33.823	13.456	13.984	19.762
Truck front view	12.984	13.945	32.503	13.045	14.679	16.84
Average	13.139	14.826	32.303	13.511	14.230	17.411
Standard deviation	0.694	0.879	4.378	0.513	0.471	1.420

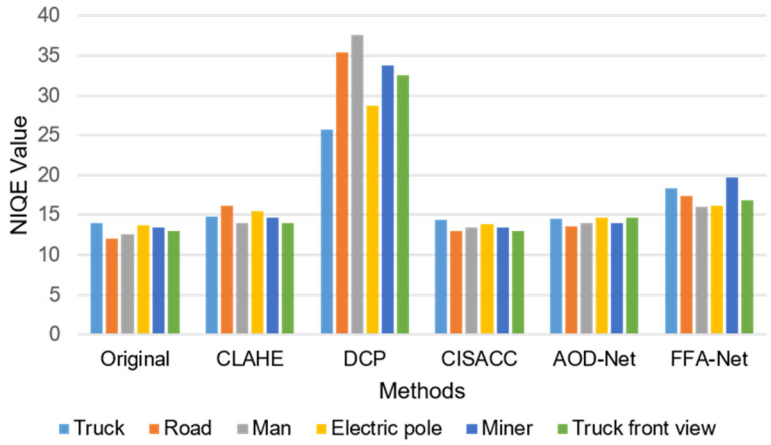

FIGURE 10 Variation of NIQE values for different methods

The transmission map was calculated, which is further related to pixel-wise depth map estimation. The mathematical representation of a haze-free image is given in Equation (4), whereas Equation (5) represents the transmission map, which is attenuated exponentially with depth in the medium:

$$J(x) = \frac{I(x) - A}{t(x)} + A, \tag{4}$$

$$t(x) = e^{-\beta d(x),} \tag{5}$$

where $J(x)$ is a haze-free image, $I(x)$ is a hazy image, A is atmospheric light, $t(x)$ is transmission map, $d(x)$ is depth map, and β is the scattering coefficient. Thus, to obtain a haze-free image, the intensity depth map should be lowered as much as possible, referring to a low-intensity depth value of the image near zero.

Figure 11 illustrates the calculated transmission maps for different methods applied to the three images. Figure 12 represents the calculated depth map of the original images and compared methods. The comparison study indicates that the CISACC method applied to the images contains a low noise. Its performance in terms of depth perception is slightly refined compared to the existing methods.

5.3 | Cumulative distribution function

Cumulative distribution function (CDF) is the probability that X's variables take a value less than or equal "*x*."

$$F(x) = Pr[X \leq x], \tag{6}$$

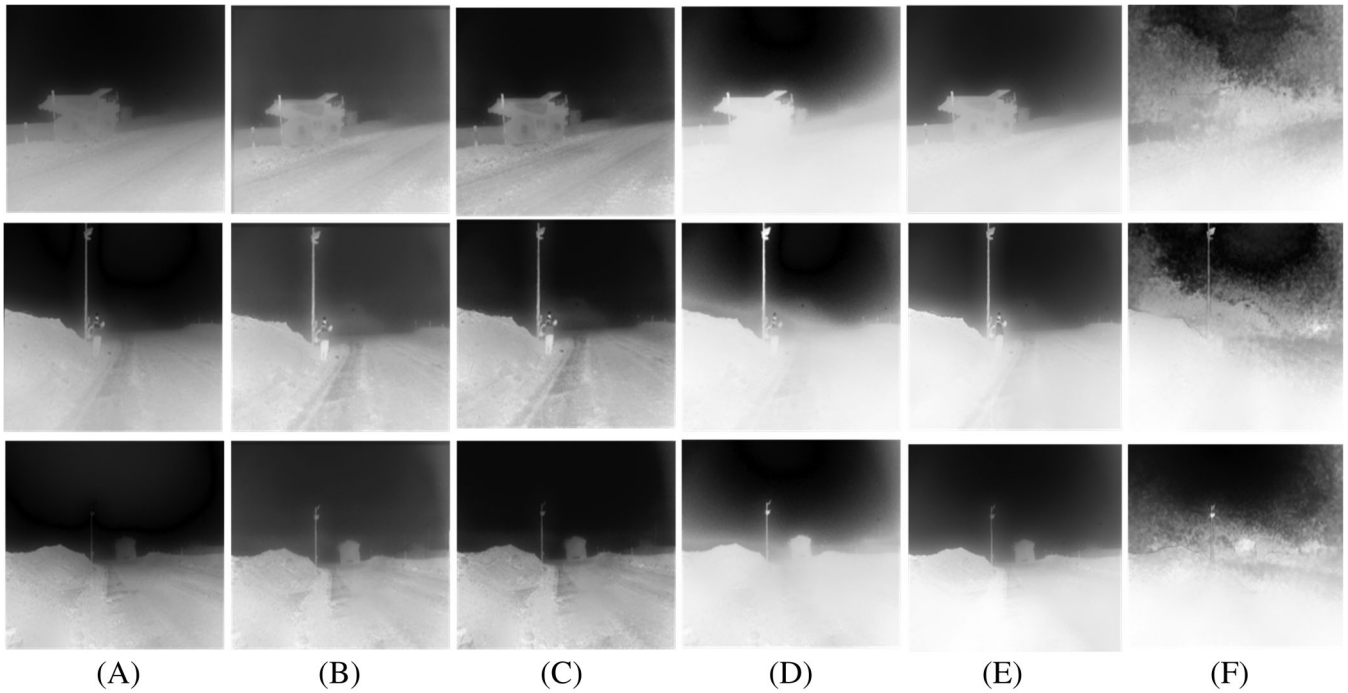

FIGURE 11 Transmission map output, (A) original image, (B) normal CLAHE image, (C) DCP image, (D) CISACC image, (E) AOD-Net image, and (F) FFA-Net image

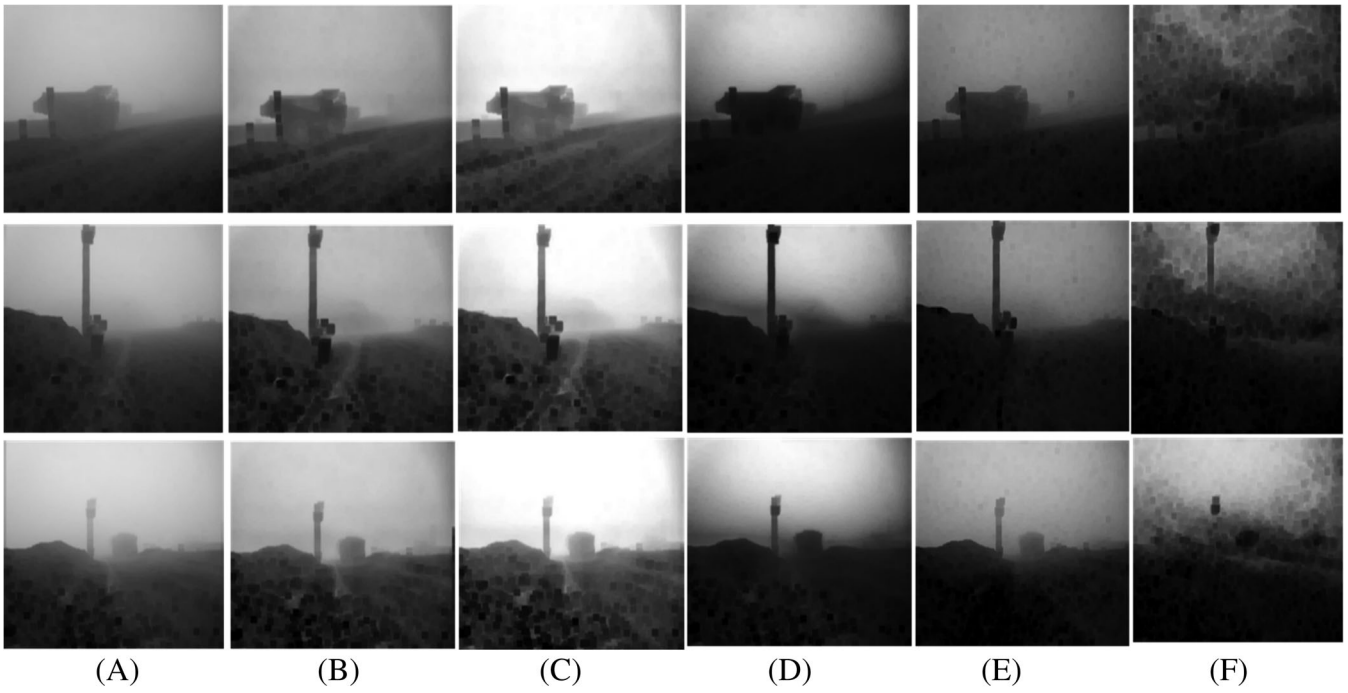

FIGURE 12 Depth map output, (A) original image, (B) normal CLAHE image, (C) DCP image, (D) CISACC image, (E) AOD-Net image, and (F) FFA-Net image

where "X" is the grayscale level and "x" is the probability of "X" of a digital image. The "x" must lie between 0–1, and "X"' should cover the whole span of a gray level from 0 to 255 for a right contrast image.

Figure 13 represents a CDF graph of the original input and output images from the normal CLAHE, DCP, CISACC, AOD-Net, and FFA-Net methods. The CISACC method has the most linear and entire span CDF, a good sign of a right contrast image.

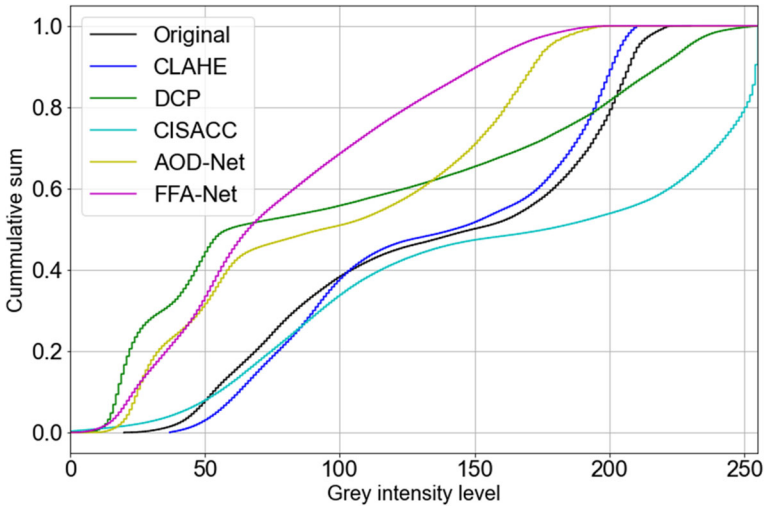

FIGURE 13 The cumulative distribution functions for the histogram of all fog removal methods

5.4 | Processing time

Evaluation of the processing time by CLAHE, DCP, CISACC, AOD-Net, and FFA-Net methods has been carried out using different original foggy images for assessing the CISACC method's efficiency. The image processing has been carried out for all the fast computing graphics processing unit (GPU) methods using Python. The resolution of the original images has been kept the same for all the methods.

Figure 14 shows the processing time taken by CLAHE, DCP, CISACC, AOD-Net, and FFA-Net methods for six hazy images, and the measured time is given in Table 3.

The normal CLAHE method has taken 0.10 s on average for processing the image, whereas DCP, CISACC AOD-Net, and FFA-Net methods have taken 0.30, 0.10, 0.87, and 1.39 s, respectively. These indicate that the CISACC method is faster than the three compared methods and almost equal to the standard CLAHE method for real-time image processing, including color correction and sharpening algorithms.

5.5 | Contrast

Contrast is the difference between higher luminance to lower luminance of an image. According to Michelson,[34] the contrast of an image is given by:

$$\text{Contrast} = \frac{I_{max} - I_{min}}{I_{max} + I_{min}}, \tag{7}$$

where I_{max} and I_{min} are the highest and lowest luminance of an image, respectively.

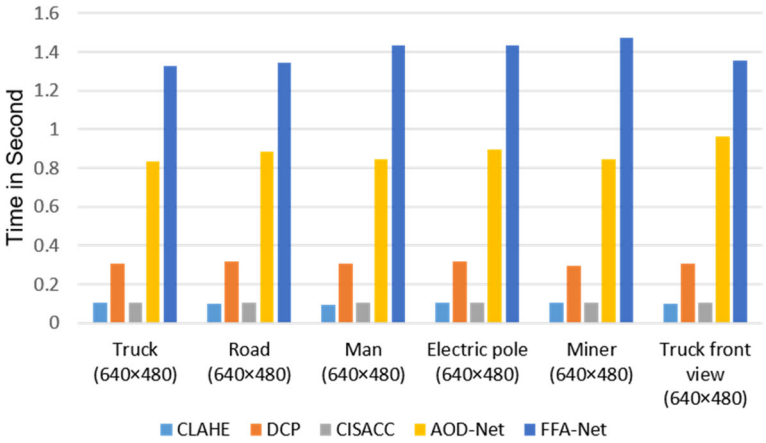

FIGURE 14 Processing time is taken by CLAHE, DCP, CISACC, AOD-Net, and FFA-Net methods for different images

TABLE 3 Image processing time taken by CLAHE, DCP, CISACC, AOD-Net, and FFA-Net methods

Test image (resolution)e	Time taken for image processing (s)				
	CLAHE	DCP	CISACC	AOD-Net	FFA-Net
Truck (640 × 480)	0.1026	0.3059	0.1059	0.8347	1.3265
Road (640 × 480)	0.1021	0.316	0.1061	0.8854	1.3423
Man (640 × 480)	0.093	0.3049	0.1025	0.8436	1.4327
Electric pole (640 × 480)	0.1027	0.3174	0.1055	0.8963	1.4357
Miner (640 × 480)	0.1047	0.2983	0.1057	0.8435	1.4728
Truck front view (640 × 480)	0.098	0.3067	0.1047	0.9641	1.3529
Average of six test values	0.100	0.308	0.105	0.877	1.3938
Standard deviation	0.004	0.007	0.001	0.04	0.06

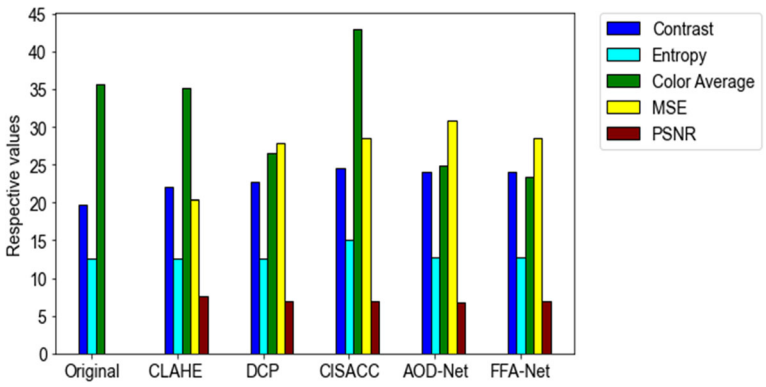

FIGURE 15 Comparative assessment for fog removal methods for average values of six images

The average contrast of six test images has been calculated for different defogging methods (Table 4); the graphical representation has been shown in Figure 15. The average contrast of six test images for the different compared methods is 0.88 for normal CLAHE, 0.91 for DCP, 0.98 for proposed CISACC, 0.96 for both AOD-Net and FFA-Net methods. However, the CISACC method has the highest average contrast value of 0.98. Further, the percentage increment of contrast has been estimated for all the compared algorithms concerning the original image contrast. It has been found that the proposed CISACC algorithm has increased the target original image's contrast by 19.28%, which is higher than the other compared methods (Table 5).

5.6 | Color average

The color average is the sum of each channel's color element of an image divided by the sum of the number of channels, which is represented as:

$$\text{Color average} = \frac{R_{\text{avg}} + G_{\text{avg}} + B_{\text{avg}}}{3}, \tag{8}$$

where R_{avg}, G_{avg}, and B_{avg} are the average of the "*R*" channel, "*G*", and "*B*" channel elements of RGB color space.

The average color value of each test image for the different dehazing algorithms has been calculated and compared with the proposed CISACC methods. The normal CLAHE, DCP, CISACC, AOD-Net, and FFA-Net methods have an average color value of 140.40, 106.25, 171.88, 99.24, and 93.17, respectively, as presented in Table 4. It has been observed that output images by the CISACC method have a better color average value for all six images. Further, the proposed CISACC algorithm has increased the target image's color average by 16.71%, a positive increment than the other dehazing methods (Table 5).

TABLE 4 Comparative assessment for fog removal methods

Test images	Methods	Contrast	Mean squared error	Color average	Peak signal-to-noise ratio (dB)	Entropy	Key point
Truck	Original	0.8	-	137.23	-	5	22
	CLAHE	0.87	59.61	137.77	30.37	5.5	336
	DCP	0.97	106.04	101.76	27.87	5	53
	CISACC	0.98	102.76	161.73	28.02	6	1582
	AOD-Net	0.97	126.98	97.34	27.09	6	24
	FFA-Net	0.95	114.06	78.84	27.55	5.96	162
Road	Original	0.9	-	149.86	-	5	768
	CLAHE	0.95	77.58	150.86	29.23	5.5	2524
	DCP	0.9	108.95	120.9	27	5	465
	CISACC	0.98	116.39	186.3	27.47	6	3155
	AOD-Net	0.97	122.79	95.05	27.23	5.93	83
	FFA-Net	0.96	115.9	82.85	27.48	6	361
Man	Original	0.78	-	131.71	-	5	238
	CLAHE	0.8	59.48	133.42	30.38	5.5	1480
	DCP	0.9	109.1	102.09	27.75	6	176
	CISACC	0.99	121.3	171.3	27.29	6.5	2338
	AOD-Net	0.95	122.01	117.94	27.26	5.89	156
	FFA-Net	0.97	109.48	117	27.73	5.93	516
Electric pole	Original	0.79	-	148.8	-	5	46
	CLAHE	0.87	107	147	30.1	5.5	1490
	DCP	0.9	118.89	109	27.3	5	34
	CISACC	0.97	113	156	28	6	2100
	AOD-Net	0.98	122.79	95.05	27.23	5.93	83
	FFA-Net	0.97	115.9	82.85	27.48	6	361
Miner	Original	0.69	-	156.2	-	5	130
	CLAHE	0.9	109	134	30.2	5	56
	DCP	0.89	115.87	107.4	27.4	5	180
	CISACC	0.99	115	170	27.9	6	1234
	AOD-Net	0.95	122.79	95.05	27.23	5.93	83
	FFA-Net	0.97	115.9	82.85	27.48	6	361
Truck front view	Original	0.8	-	130.5	-	5	158
	CLAHE	0.89	76.8	139.4	30.6	5	1456
	DCP	0.92	111.4	96.4	27.6	6	118
	CISACC	0.99	115.9	186	27.9	6.5	2345
	AOD-Net	0.98	122.79	95.05	27.23	5.93	83
	FFA-Net	0.99	115.9	82.85	27.48	6	361
Average	Original	0.793333	-	142.383	-	5	227
	CLAHE	0.88	81.578	140.408	30.146	5.333	1223.667
	DCP	0.913333	111.708	106.258	27.486	5.333	171
	CISACC	0.983333	114.058	171.888	27.763	6.166	2125.667
	AOD-Net	0.966667	123.358	99.246	27.211	5.935	85.333
	FFA-Net	0.968	114.06	93.173	27.533	5.981	353.666

TABLE 5 Comparative increment assessment for fog removal methods in percentage

Test images	Methods	Contrast increment w.r.t original (%)	Contrast increment of CISACC w.r.t other methods (%)	Color average increment w.r.t original (%)	Color average increment of CISACC w.r.t other methods (%)	Entropy increment w.r.t original (%)	Entropy increment of CISACC w.r.t other methods (%)
Truck	CLAHE	8.04		0.39		9	
	DCP	17.52		−25.84		0	
	CISACC	18.36		15.14		16.6	
	AOD-Net	17.52		−29.06		16.66	
	FFA-net	15.78		−42.54		16.16	
Road	CLAHE	5.2		0.66		9	
	DCP	0		−19.3		0	
	CISACC	8.16		19.55		16.6	
	AOD-Net	7.21		−36.57		16	
	FFA-net	6.25		−44.71		16.66	
Man	CLAHE	2.5		1.28		9	
	DCP	13.3		−22.48		16.6	
	CISACC	21.21		23.11		23	
	AOD-Net	17.8		−10.45		15.11	
	FFA-net	19.58		−11.16		15.68	
Electric pole	CLAHE	9.19		−1.2		9.09	
	DCP	12.2		−26.74		0	
	CISACC	18.5		4.6		16.6	
	AOD-Net	19.38		−36.12		15.68	
	FFA-net	18.55		−44.32		16.66	
Miner	CLAHE	23.3		−14.21		0	
	DCP	22.47		−31.24		0	
	CISACC	30.3		8.11		16.6	
	AOD-Net	27.36		−39.14		15.68	
	FFA-net	28.86		−46.95		16.66	
Truck front view	CLAHE	10.11		6.38		0	
	DCP	13		−26.8		16.6	
	CISACC	19.19		29.8		23.07	
	AOD-Net	18.36		−27.16		15.68	
	FFA-net	19.19		−36.51		16.66	
Overall increment (%)	CLAHE	9.723	9.563	1.116	15.601	6.015	12.73
	DCP	13.081	6.205	−25.4	42.118	8.3	10.445
	CISACC	19.286		16.718		18.745	
	AOD-Net	17.8	1.486	−29.75	46.468	15.801	2.943
	FFA-net	18.035	1.251	−37.698	54.416	16.413	2.331
	Average		4.626		39.65		7.112

5.7 | Mean squared error and peak signal to noise ratio

Mean squared error (MSE), and peak signal to noise ratio (PSNR) is the error metrics to measure the image quality concerning the original foggy image. The MSE is the cumulative squared error to the enhanced image and the original hazy image, whereas PSNR measures the peak error.[35] The lesser the value of MSE, the lower the error.[14] MSE is calculated as:

$$\mathrm{MSE} = \frac{\sum_{\mathrm{M,N}} [I_1(m,n) - I_2(m,n)]^2}{\mathrm{M} \times \mathrm{N}}, \tag{9}$$

where M is the number of rows, and N is the number of columns in the image.

The higher the PSNR, the better the enhancement of the image.[35] The PSNR is calculated as:

$$\mathrm{PSNR} = 10 \log_{10}\left(\frac{R^2}{\mathrm{MSE}}\right), \tag{10}$$

where R is the maximum fluctuation in the input image. If it has an 8-bit unsigned integer image data, then R is 255.

The MSE values are 81.5 for CLAHE, 111.7 for DCP, 123.3 for AOD-Net, and 114.0 for FFA-Net, whereas the proposed CISACC has a 114.0 MSE value lower contrast than the AOD-Net method only. The PSNR values are 30.1 for CLAHE, 27.48 for DCP, 27.21 for AOD-Net, and 27.5 for FFA-Net; conversely, the proposed CISACC has 27.76 (Table 4). In general, an improved image is easily acceptable by human perception when its PSNR is more than 30 dB.[35] The proposed method has a slightly better PSNR value than the other compared methods except for the normal CLAHE. This is the limitation of the proposed method.

5.8 | Entropy

The image's entropy is the randomness or heterogeneity of states of the image. If the image is perfectly histogram equalized and the spread of states is the maximum, its entropy will be high, whereas the limited states' entropy is low. The entropy "H" of an image is given by:

$$H = \sum_{k=0}^{M-1} (P_k \log_2(P_k)), \tag{11}$$

where M is the number of gray levels, P_k is the histogram count of gray level k.

The proposed CISACC method has the highest heterogeneity. Hence, the features are more visible than normal CLAHE. The entropy of an image is directly proportional to the information contained in the image.[14] Figure 16 represents the original input image's entropy and output images of the normal CLAHE, DCP, CISACC, AOD-Net, and FFA-Net methods. The CISACC method has an average entropy of 6.1, both CLAHE and DCP methods have an average entropy of 5.3, and both AOD-Net and FFA-Net methods have 5.9 for the six test images (Table 4). Thus, the proposed CISACC algorithm has high information content as its entropy has increased for the targeted image by 18.7%, which is higher than all the compared methods (Table 5).

5.9 | Feature keypoint

Feature keypoint include edges, corners, blobs, and any interest points of an image. Koonsanit et al.[10] used the scale-invariant feature transform (SIFT) feature key point detector to assess the image's visibility, which depends on the prominence of features of the image. The higher the detected

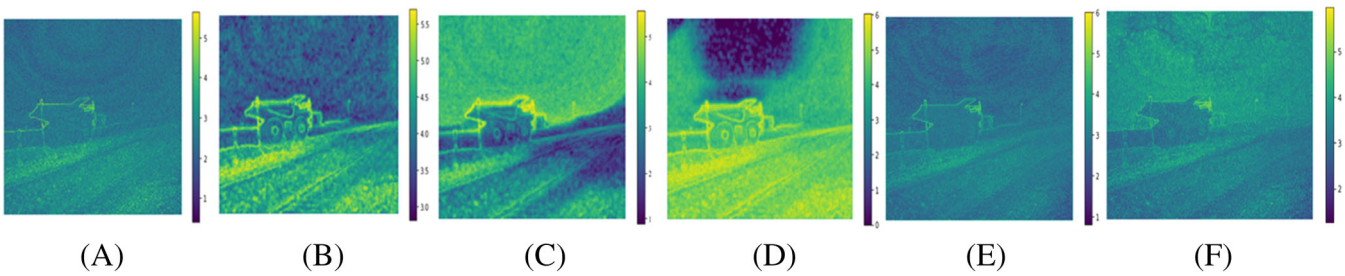

FIGURE 16 Entropy map, (A) original image, (B) CLAHE method, (C) DCP method, (D) CISACC method, (E) AOD-Net, and (F) FFA-Net

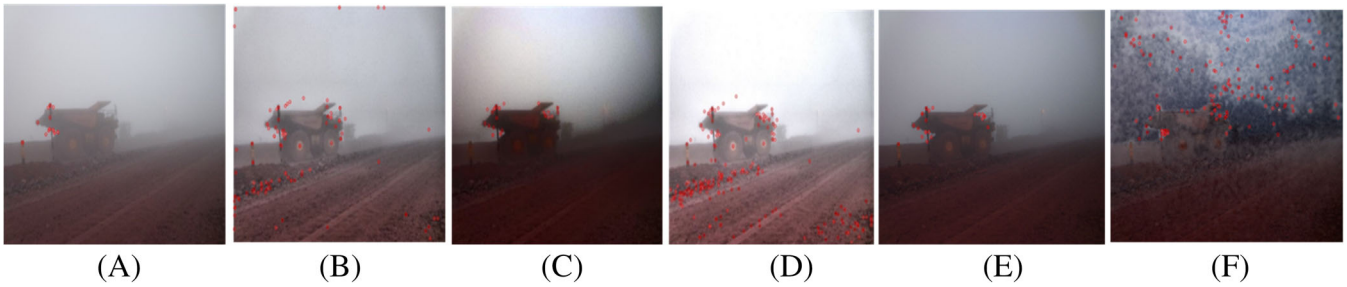

FIGURE 17 Feature keypoint maps, (A) original image keypoint map, (B) normal CLAHE keypoint map, (C) DCP keypoint map, (D) CISACC keypoint map, (E) AOD-Net keypoint map, and (F) FFA-Net keypoint map

key points, the better the visibility of the image. Feature keypoints' detection has been carried out using the SIFT in Python (OpenCV) to quantify image clarity.

Figure 17 illustrates the feature key point on the original input image and the processed images from normal CLAHE, DCP, CISACC, AOD-Net, and FFA-Net methods. It has been observed that the CISACC image has a higher number of feature key points (2125.6) than the normal CLAHE (1223.6), DCP (171), AOD-Net (85.3), and FFA-Net (353.6) methods (Table 4).

5.10 | Comparison of CISACC with other existing dehazing techniques

To evaluate the advantages of the proposed method (CISACC) over other image dehazing techniques developed by different researchers, a features comparison of all existing methods has been given in Table 6. Some current methods include dark channel prior (DCP),[33] CLAHE,[11,12,15,22] AOD-Net,[20] FFA-Net,[21] underwater image enhancement,[36] pyramid dehazing network,[37] NIN-DehazeNet,[38] and so forth.

TABLE 6 Comparative analysis of the proposed technique with the existing image dehazing techniques

Features	Dark Channel Prior method (He et al.[34])	CLAHE (Bandara et al.,[12] Koonsanit et al.,[22] Maxwell et al.,[11] Ramya,[15] Smitha et al.[16])	AOD-Net (Li et al.[20])	FFA-Net (Qin et al.[21])	Underwater Image Enhancement (Cai et al.[36])	Pyramid Dehazing Network (Zhang et al.[37])	NIN-DehazeNet (Yuan et al.[38])	Proposed technique (CISACC)
Real-time color restoration	×	✓	×	×	×	×	×	✓
Application of convolutional neural network	×	×	✓	✓	✓	✓	✓	×
Low computational complexity	×	✓	×	×	×	×	×	✓
Enhancement of low illuminated pixels and restoration of dehaze image	✓	×	✓	×	✓	✓	✓	✓
No requirement of estimation of transmission map and atmospheric light to get dehaze image	×	✓	×	×	×	×	×	✓
No requirement of huge amount of past training data	✓	✓	×	×	×	×	×	✓
Less processing time for real-time implementation	×	×	×	×	×	×	×	✓
Histogram equalization	×	✓	×	×	×	×	×	✓
Algorithm works without high processing GPU	×	✓	×	×	×	×	×	✓

The existing approaches work only for the nonsky patches. The estimation of transmission map and atmospheric scattering light becomes difficult for high foggy areas; thus, there is room for error while dealing in real practical situations. One of the significant drawbacks of these existing techniques is that they deteriorate the natural color of the images during real-time processing. From Table 6, it can be analyzed that the proposed method has some advantages compared to the other existing techniques. The proposed method does not use convolutional neural networks to enhance the image, thus decreasing complexity during computation. However, the primary advantage of the CISACC algorithm is that it displays the low illuminated pixels, and it restores the natural color of the image in real-time.

The primary work function of the proposed algorithm includes virtual histogram stretching (0–255 intensity values), frequency normalization using a fixed threshold level, and eventually equalizing the histogram value, which provides better contrast of the image and increases low-light features. It restores color by balancing the blue, green, and red (BGR) values, also known as the white balance. It does not generate a transmission map and estimates atmospheric light, saving most of the processing time compared to the other techniques. This serves as a significant advantage compared to other image dehazing techniques. While most algorithms operate on vast preobtained data of all environmental conditions, the CISACC method does not require previous data to enhance the image.

One of the basic features required for real-time implementation of the technique is its processing speed, requiring high processing GPU. As the proposed algorithm does satisfactory work without the need for this high processor, it can be said that the algorithm is suitable for working in real-time at opencast mine sites. Therefore, the CISACC method has more features among the eight methods as compared in Table 6.

6 | CONCLUSIONS

The drivers are unable to drive due to low visibility in opencast mining areas during foggy weather. Sometimes, the limited field of view for HEMM operators causes vehicles to derail, increasing the risk of accidents. An integrated vision enhancement system has been developed to solve the above problems, including 180° panorama stitching, real-time object detection, and an integrated image processing technology (CISACC). The system also incorporates proximity warning devices using radar, navigation through 3D geo-tagged mine map using GNSS, fleet management software, and other devices for providing multistage safety during driving in foggy weather. The characteristics of the entire system have been compared with other existing systems. Significantly, the fogy image enhancement algorithm has also been compared with the proposed image enhancement algorithms. The proposed system is a complete solution to the visibility problem due to fog in opencast mining areas. The combination of hardware and software of the whole system makes it unique from the existing systems. In addition, the proposed image enhancement method has been compared with other existing methods, and it is found that the various evaluation parameters of the proposed method are superior to the existing methods.

The NIQE value has been calculated to measure the image distortion. The CISACC method has less distortion than the normal CLAHE, DCP, AOD-Net, and FFA-Net methods, as the NIQE values are 14.8, 32.3, 14.2, and 17.4, respectively, while the CISACC has 13.5. It is also observed that the proposed CISACC algorithm has increased contrast, entropy, and color averaging. The contrast percentage increase of the proposed method is 9.56%, 6.20%, 1.48%, and 1.25%, respectively, over the normal CLAHE, DCP, AOD-Net, and FFA-Net methods.

The proposed method successfully preserved the colors of the image, although the image went through a considerable histogram equalization. The percentage increase in CISACC's color average is 15.60%, 42.11%, 46.46%, and 54.4% compared to the common CLAHE, DCP, AOD-Net, and FFA-Net methods, respectively. The information contained in the proposed method is also higher than the other existing methods. The percentage increment in entropy of the proposed method is 12.7%, 10.4%, 2.94%, and 2.33% than the common CLAHE, DCP, AOD-Net, and FFA-Net methods, respectively. Further, the CISACC method increases the overall feature key points in the processed image. The normal CLAHE has 1223.6 feature key points, DCP has 171, AOD-Net has 85.3, and FFA-Net has 353.6 feature key points, while CISACC has a total of 2125.6 key points. Also, the processing time of CISACC is better than comparable methods except for normal CLAHE. The developed intelligent vision enhancement system also provides a 180° panorama view of three stitched videos to increase the driver's field of view. For detecting the mining field's upcoming obstacle, an object detection algorithm is used using CNN with an accuracy of 97% with boundary boxing. Hence, the developed vision enhancement system and CISACC method may improve real-time images in foggy weather.

However, the main limitation of the CISACC method is that it produces a halo effect in the sky part during dense fog that can be analyzed by applying a different algorithm to the sky part after dividing the sky, which can be done in future work. The proposed method works in real-time. Therefore, the system can be accelerated by building it on a dedicated field-programmable gate array (FPGA) to reduce processing time. The PSNR is less than 30 dB which can be improved by optimizing the proposed algorithm for applications in foggy image enhancement. Additionally, external infrared illuminators may be used to assist the proposed system for better visibility through the dense fog.

ACKNOWLEDGMENTS

The authors are grateful to Dr. P. K. Singh, Director, CSIR-Central Institute of Mining and Fuel Research, Dhanbad, India, for his valuable guidance and granting permission to publish this article. The authors are also indebted to the Ministry of Electronics and Information Technology, Government of India, and National Mineral Development Corporation Limited, Hyderabad, India, for sponsoring the project with grant no. 16 (1)/2018-ESDA.

DATA AVAILABILITY STATEMENT

The datasets generated during and/or analyzed during the current study are available from the corresponding author on reasonable request.

ORCID

Sushma Kumari https://orcid.org/0000-0002-7784-4979
Swades Kumar Chaulya https://orcid.org/0000-0002-5396-0086

REFERENCES

1. Saurabh K, Chaulya SK, Prasad GM, Ansari S, Kumar D. Assessment of different technologies for improving visibility during foggy weather in mining and transportation sectors. *Int J Recent Innov Trends Comput Commun (IJRITCC)*. 2016;4(4):31-40. https://doi.org/10.17762/ijritcc.v4i4.1949
2. Chatterjee D, Chaulya SK. Vision improvement system using image processing technique for adverse weather condition of opencast mines. *Int J Min Reclam Environ*. 2019;33(7):505-516.
3. Wei Z, Jun W, Lidong H, Zebin S. Combination of contrast limited adaptive histogram equalisation and discrete wavelet transform for image enhancement. *IET Image Process*. 2015;9(10):908-915. https://doi.org/10.1049/iet-ipr.2015.0150
4. Mohanram S, Aarthi B, Silambarasan C, Hephzibah TJS. An optimised image enhancement of foggy images using gamma. *Int J Adv Res Electron Commun Instrum Eng Dev*. 2014;3(2):155-159.
5. Saxena A, Saxena R, Pandey Y. An exhaustive analysis on various foggy image enhancement techniques. *Int J Adv Res Comp Sci Electron Eng*. 2014;3(1):11-17.
6. Abbaspour MJ, Yazdi M, Shirazi MM. A new fast method for foggy image enhancement. Shīrāz D-i, ed. *Proceedings of the IEEE Iranian Conference on Electrical Engineering (ICEE)*. IEEE; 2016:1855-1859. https://doi.org/10.1109/IranianCEE.2016.7585823
7. Ravikiran JS, Gotham M. Fog image enhancement using DWT. *Int J Innov Res Comput Commun Eng*. 2016;4:14436-14441.
8. Sangeetha N, Anusudha K. Image defogging using enhancement techniques. Salivahanan S, ed. *Proceedings of IEEE International Conference on Communication and Signal Processing (ICCSP)*. IEEE; 2017:10-11. https://doi.org/10.1109/ICCCSP.2017.7944087
9. Qiu J, Li HH, Zhang T, Ma F, Yang D. Automatic x-ray image contrast enhancement based on parameter auto-optimisation. *J Appl Clin Med Phys*. 2017;18(6):218-223.
10. Koonsanit K, Thongvigitmanee S, Pongnapang N, Thajchayapong P. Image enhancement on digital x-ray images using n-CLAHE. Sidky EY, ed. *Proceedings of 10th IEEE Transactions on Biomedical Engineering (T-BME)*. IEEE; 2017:1-4. https://doi.org/10.1109/BMEiCON.2017.8229130
11. Maxwell EG, Tripti C. A comparison between contrast limited adaptive histogram equalisation and Gabor filter sclera blood vessel enhancement techniques. *Int J Soft Comput Eng*. 2013;3(4):22-25.
12. Bandara AMRR, Kulathilake KASHK, Giragama PWGR. Super-efficient spatially adaptive contrast enhancement algorithm for superficial vein imaging. Ranaweera R, ed. *Proceedings of 10th IEEE International Conference on Industrial and Information Systems (ICIIS)*. IEEE; 2017:1-6. https://doi.org/10.1109/ICIINFS.2017.8300427
13. Setiawan AW, Mengko TR, Santoso OS, Suksmono AB. Color retinal image enhancement using CLAHE. Supangkat SH, Lim C-S, eds. *Proceedings of IEEE International Conference on ICT for Smart Society (ICISS)*. IEEE; 2013:1-3. https://doi.org/10.1109/ICTSS.2013.6588092
14. Ma J, Fan X, Yang SX, Zhang X, Zhu X. Contrast limited adaptive histogram equalization-based fusion in YIQ and HSI color spaces for underwater image enhancement. *Int J Pattern Recognit Artif Intell*. 2018;32(7):1854018. https://doi.org/10.1142/S0218001418540186
15. Ramya C, Rani SS. A novel method for the contrast enhancement of fog degraded video sequences. *Int J Comput Appl*. 2012;54(13):1-5.
16. Smitha N, Ujwala BS, Manjunatha P, Chethan LS. Contrast limited adaptive histogram equalisation and discrete wavelet transform method used for image. *Int J Res Trends Innov*. 2017;2(8):142-146.
17. Kim K, Kim S, Kim KS. Effective image enhancement techniques for fog-affected indoor and outdoor images. *IET Image Process*. 2018;12(4):465-471. https://doi.org/10.1049/iet-ipr.2016.0819
18. Lv X, Chen W, Shen I. *Real*-time dehazing for image and video. Cohen-Or D, Bao H, eds. *Proceedings of IEEE 18th Pacific International Conference on Computer Graphics and Applications (ICCGA)*. IEEE; 2010:62-69. https://doi.org/10.1109/PacificGraphics.2010.16
19. Zhu MZ, He BW, Zhang LW. Atmospheric light estimation in hazy images based on color-plane model. *Comput Vis Image Underst*. 2017;165:33-42. https://doi.org/10.1016/j.cviu.2017.09.005
20. Li B, Peng X, Wang Z, Xu J, Feng D. AOD-net: all-in-one dehazing network. Ikeuchi K, Medioni G, Pelillo M, eds. *Proceedings of International Conference on Computer Vision*. IEEE; 2017:4780-4788. https://doi.org/10.1109/ICCV.2017.511
21. Qin X, Wang Z, Bai Y, Xie X, Jia H. FFA-net: feature fusion attention network for single image dehazing. Rossi F, ed. *Proceedings of 34th Conference on Artificial Intelligence(CAI)*. AAI Press, Palo Alto, California, USA; 2019:11909-11915. https://arxiv.org/abs/1911.07559
22. Nieto A, Sun E, Li ZX. Real-time assisted driving in open pit mining operations using Google earth. *Miner Eng*. 2010;62:21-26.
23. Sun E, Zhang X. 3D assisted driving system for haul trucks in surface mining. Dong W, ed. *Proceedings of International Conference on Transportation, Mechanical, and Electrical Engineering (TMEE)*. IEEE; 2011:363-366. https://doi.org/10.1109/TMEE.2011.6199218
24. Spinneker R, Koch C, Park S, Yoon JJ. Fast fog detection for camera-based advanced driver assistance systems. Eskandarian A, ed. *Proceedings of 17th IEEE Transactions on Intelligent Transportation Systems (T-ITS)*; Qingdao: IEEE; 2014:1369-1374. https://doi.org/10.1109/ITSC.2014.6957878
25. Nieto A, Dagdelen K. Development of dump edge and vehicle proximity warning system using GPS and wireless network communications to improve safety in open pit mines. Proceedings of the SME Annual Meeting; 2002:1-8; Phoenix. https://www.researchgate.net/publication/332071490
26. Ruff T. Evaluation of a radar-based proximity warning system for off-highway dump trucks. *Accid Anal Prev*. 2006;38:92-98. https://doi.org/10.1016/j.aap.2005.07.006
27. Xiao D, Li H, Ji Z, Xu E, Luo B, Chen J. An anti-collision early warning system for mine trucks based on RBF network and WIFI. *J Phys Conf Ser*. 1631;2020(1):012157. https://doi.org/10.1088/1742-6596/1631/1/012157
28. Limare N, Lisani J, Morel J, Bel A. Simplest color balance algorithm implementation. *IPOL Image Process*. 2011;1:297-315. https://www.ipol.im/pub/art/2011/llmps-scb/?utm_source=doi
29. Kaur H, Sohi N. A study for applications of histogram in image enhancement. *Int J Eng Sci*. 2017;6(6):59-63. https://doi.org/10.9790/1813-0606015963

30. Pal K, Patel BV. Data classification with k-fold cross-validation and holdout accuracy estimation methods with 5 different machine learning techniques. Baraneetharan E, ed. *Proceedings of 4th International Conference on Computing Methodologies and Communication (ICCMC)*. IEEE; 2020:83-87. https://doi.org/10.1109/ICCMC48092.2020.ICCMC-00016
31. Mittal A, Sundararajan R, Bovik AC. Making a completely blind image quality analyser. *IEEE Signal Process Lett*. 2013;22(3):209-212. https://doi.org/10.1109/LSP.2012.2227726
32. Zhang S, Yao J & Re WL Single image haze removal via joint estimation of detail and transmission. Proceedings of International Conference on Multimedia & Expo Workshops (ICMEW); 2018:1-6. https://doi.org/10.1109/ICMEW.2018.8551504.
33. He K, Sun J, Tan X. Single image haze removal using dark channel prior. *IEEE Trans Pattern Anal Mach Intell* 2011; 33(12):2 341–2353.
34. Michelson A. *Studies in Optics*. University of Chicago Press; 1927:21-33.
35. Sara U, Akter M, Uddin MS. Image quality assessment through FSIM, SSIM, MSE and PSNR—a comparative study. *J Comput Commun*. 2019;7(3):8-18. https://doi.org/10.4236/jcc.2019.73002
36. Cai C, Zhang Y, Liu T. Underwater image processing system for image enhancement and restoration. Othman JB, ed. *Proceedings of IEEE 11th International Conference on Communication Software and Networks (ICCSN)*; 2019:381-387. https://doi.org/10.1109/ICCSN.2019.8905310
37. Zhang H, Patel VM. Densely connected pyramid dehazing network. Brown MS, Morse B, Peleg S, eds. *Proceedings of IEEE Conference on Computer Vision and Pattern Recognition (CVPR)*. IEEE; 2018:3194-3203. https://doi.org/10.1109/CVPR.2018.00337
38. Yuan K, Wei J, Lu W, Xiong N. Single image dehazing via NIN-DehazeNet. Olague G, ed. *IEEE Access*. Vol 7; 2019:181348-181356. https://doi.org/10.1109/ACCESS.2019.2958607

How to cite this article: Kumari S, Choudhary M, Mishra R, et al. Artificial intelligent based smart system for safe mining during foggy weather. *Concurrency Computat Pract Exper*. 2021;e6631. https://doi.org/10.1002/cpe.6631